

MASTERTHESIS

SCRIPT

**VARIABILITY OF UPPER OCEAN
HEAT CONTENT IN THE NORTH
ATLANTIC**

September 19, 2013

Martin Moritz

¹⁰ University of Hamburg

martin.moritz@zmaw.de

Abstract

Contents

1	Introduction	3
1.1	Heat in the Ocean	3
1.2	Studies on global HC and regional variations	7
5	1.3 Current system and water masses in the study area	10
	1.4 Aim and structure of this study	11
2	Data and Methods	13
10	2.1 Study area	13
	2.2 eXpandableBathyThermograph (XBT)	15
	2.2.1 Probe design and operation	16
	2.2.2 Bias	17
15	2.3 Calculation of Heat content	20
	2.3.1 Heat content relative to a fixed depth	20
	2.3.2 Heat content relative to a fixed isotherm	21
	2.4 Gridding	22
	2.4.1 Barnes interpolation scheme	23
	2.4.2 DIVA scheme	24
	2.4.3 Application and performance of interpolation	25
3	Results	34
20	3.1 Temperature Section	34
	3.2 HC time-series on the reference section	36
	3.3 Horizontal maps	38
	3.4 HC relative to fixed isotherm	41
	3.5 HC and NAO	44
25	4 Summary and Discussion	45

1 Introduction

In this study the temporal and spatial evolution of the upper ocean heat content (HC) in the North Atlantic along the frequently repeated section AX 3 is analysed. The dataset consists of temperature data from eXpandable BathyThermographs (XBTs) for the period 1988-2012. This chapter will give an overview of how the ocean gains and loses heat, of the importance of monitoring HC and its changes and how this can be accomplished from temperature measurements. Furthermore results of previous studies are summarised, the characteristics of the current system in the study area and the aims of this study are outlined.

1.1 Heat in the Ocean

At the surface the ocean gains heat through incoming solar shortwave radiation Q_{SW} . The amount and distribution of Q_{SW} varies with season, time of the day, latitude and cloud cover. It is largest at tropical regions. The oceans loss of heat is determined by different processes. It is largest through latent heat fluxes Q_L , which are most intense in subtropical regions. Here the cloud cover is low and strong dry winds blow from the continents and increase the flux of heat by evaporating water. The flux of long-wave radiation Q_{LW} out of the ocean is largest in areas of low cloud cover, basically in the subtropical regions and centers of the oceans. The sensible heat flux Q_S due to conduction is the smallest component making a contribution to the total heat loss. It is largest during winter and in regions where intense cold winds blow from the continents and large air-sea temperature differences occur.

The net heat exchange through the air-sea-boundary layer is the sum of these fluxes and in a zonal average there is a net energy gain of the ocean at low latitudes and a net energy loss at high latitudes (see Fig. 1) - the ocean is heated in

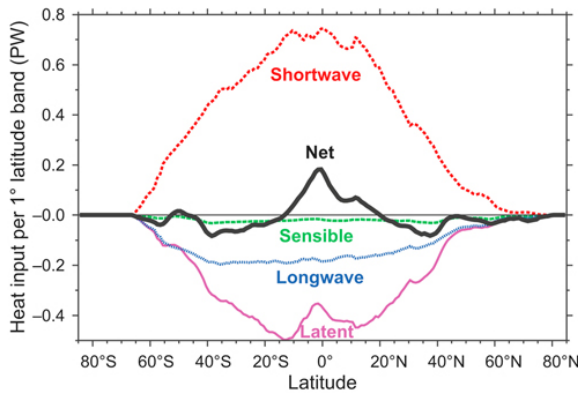


Fig. 1: Components of total heat flux contributing to the net heat flux through the ocean surface as a function of latitude. At the tropics the ocean warms whereas at higher latitudes the ocean loses heat (Talley et al., 2011)

the tropics and cooled at the poles. If the net air-sea heat flux is positive, heat is mixed into the upper layer of the ocean by wind-induced turbulence (Olbers et al., 2012). Due to the oceans high heat capacity a huge amount of heat can be stored and transported by currents, away from the tropics and subtropics to higher latitudes. The main factors that determine the heat transport are the wind driven circulation (Ekman-transports), geostrophic currents and the Meridional Overturning Circulation (MOC). The largest amount of heat is released at the poleward ends of the western boundary currents (e.g. Gulf Stream, Kuroshio) and at polar and subpolar latitudes where warm water comes into contact with cold air (Vallis, 2012)(see Fig. 2).

In the North Atlantic Heat is transported northwards by the Gulf Stream (GS), the North Atlantic Current (NAC) and its several branches. As it is released to the atmosphere it moderates the climatic conditions in Europe. Thus, the oceans ability to store and to transport heat has important impacts on climate on regional and also global scales. Furthermore, the ocean is able to buffer temperature rise. As it takes up heat from the atmosphere it may reduce the warming at the surface

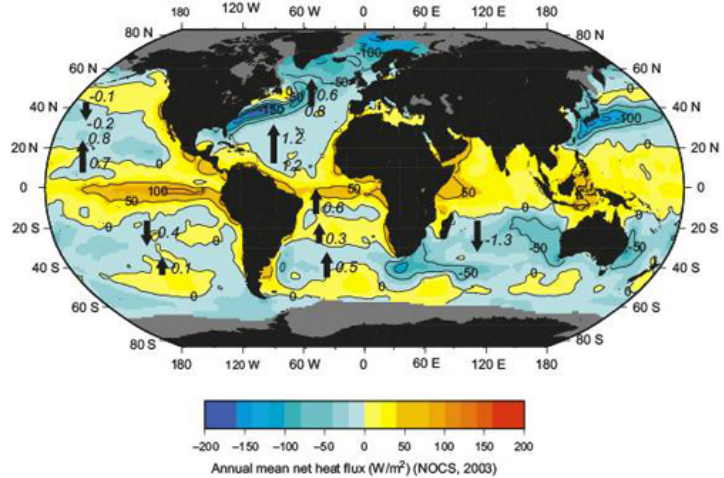


Fig. 2: Annual mean net heat fluxes in $\frac{\text{W}}{\text{m}^2}$. The arrows show the meridional heat transports in PW. A net gain in heat occurs within the tropical regions, whereas at higher latitudes there is a net heat loss, which is greatest at the western boundary currents and the Nordic Seas. (Talley et al., 2011)

which is induced by the back radiation of long-wave radiation caused by greenhouse gases. There is also a close relationship between the oceanic sea-level and ocean heat content. As seawater warms, its density decreases and expands. The increase in volume results in an increase of sea-level. About half of the changes in sea-level can be attributed to changes in thermal expansion due to warming of the ocean (Talley et al., 2011). Thus, monitoring the change in ocean HC is important as it reveals information about changes in climatic conditions and the thermosteric contribution to sea level changes.

To understand how to measure changes in HC one may consider a column of seawater. The total change of heat within this column is determined by the sum of advective fluxes by currents (Q_{adv}), the net surface heat fluxes (Q_{surf}) and some residual fluxes (Q_{res}) arising from diapycnal mixing and diffusion processes (see Fig. 3):

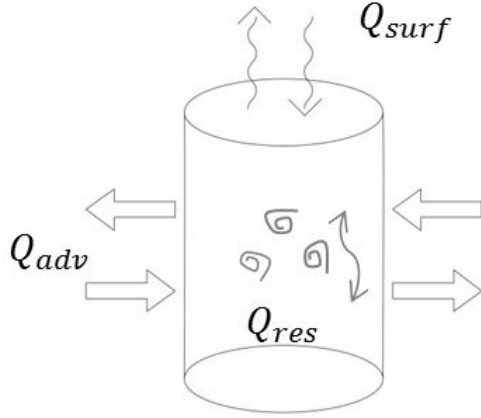


Fig. 3: Scheme depicting the advective Q_{adv} , surface heat fluxes Q_{surf} and fluxes due to mixing and diffusion processes Q_{res} as the main contributors to the change of heat content within a column of water.

$$\frac{\partial HC}{\partial t} = Q_{adv} + Q_{net} + Q_{res} \quad (1)$$

The heat content itself can be estimated as the vertical integral of temperature (T) minus a reference temperature (T_{ref}) and multiplied by the density (ρ) and specific heat (c_p) of sea water:

$$HC = c_p \rho \int (T - T_{ref}) dz \quad (2)$$

By measuring T , assuming ρ and c_p are known, and estimating the HC and its change, it is possible to detect warming or cooling signals of the ocean. Estimates in HC change can be used to investigate physical mechanisms that cause this deviation from a mean state, e.g. changes in Earth's heat budget, and how these impact climatic conditions.

1.2 Studies on global HC and regional variations

Earlier studies, eg. by *Domingues et al.* (2008); *Gouretski and Reseghetti* (2010), of the global ocean HC show a significant warming signal. The estimates of ocean HC anomalies depicted in Fig 4. show a high interannual variability and besides the positive trend, the estimates differ among themselves. These differences occur due to the use of different datasets, quality controls, assumptions made to fill areas of missing data (e.g. averaging and interpolation methods), climatologies and corrections of instrumental biases.

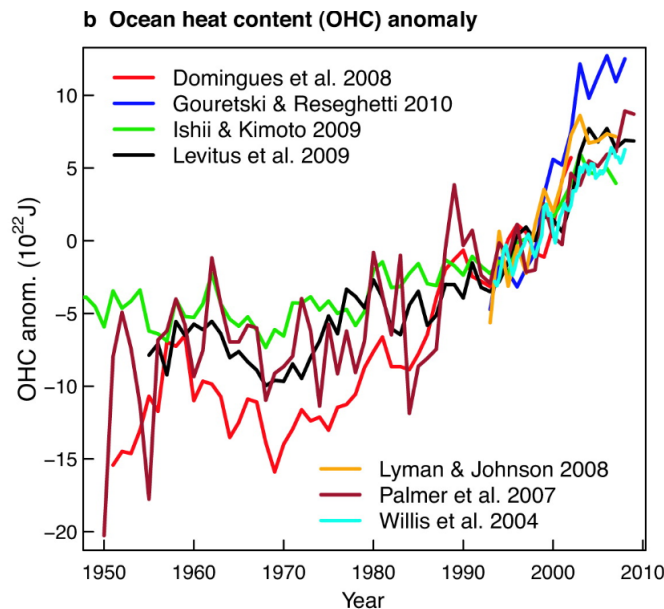


Fig. 4: Different estimates of global ocean heat content anomalies. The differences occur due to different methodologies, e.g. different reference values. All show a warming signal of the global ocean. (Pierce et al., 2011)

According to *Levitus et al.* (2012) the greatest contribution of the warming signal between 1955-2010 is from the Atlantic Ocean and in particular the North Atlantic (see Fig. 5). They state the warming is most intense in the surface layers and below the 100 m layer the Atlantic exhibits the largest increase of HC of

all ocean basins. According to their calculations the upper ocean accounted for approximately two-third of the warming of the 0-2000 m layer of the ocean.

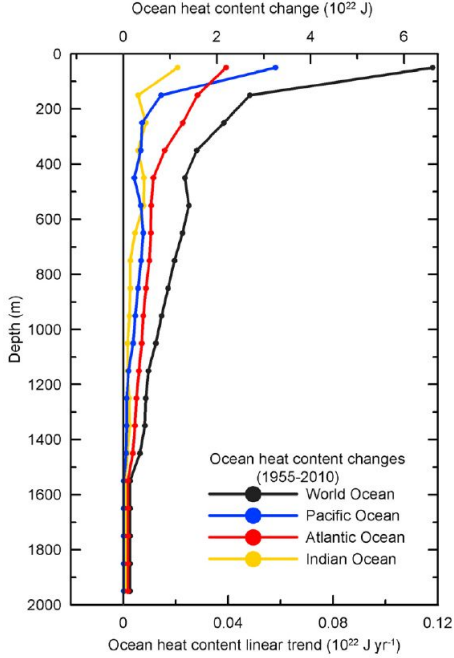


Fig. 5: Linear trend and total increase of ocean basin heat content based on the linear trend of global and individual basins as a function of depth (0-2000m) for 100 m thick layers. Within the upper layers the Atlantic has the largest contribution to ocean heat content changes (Levitus et al., 2012)

The signal of HC change is not uniformly distributed but may vary regionally. *Zhai and Sheldon (2012)* analysed the HC change of the upper 0-700 m between the periods 1955-70 and 1980-95 and *Lozier et al. (2008)* investigated the spatial variability of HC in the North Atlantic basin between the periods 1950-1970 and 1980-2000 . They compared observational data with the results of model experiments. Both found a similar spatial pattern of HC change with warming in the tropics and subtropics and cooling in the subpolar ocean (see Fig 6). These regional variations in HC may arise from processes occurring on different temporal

and spatial scales. Important contributors are changes in advection of heat by wind-driven currents and mesoscale eddy activity, changes in net heat and freshwater fluxes, changes in strength and shifts of gyre circulation.

Eden and Willebrand (2001) found in their model studies that the dominant part of the North Atlantic variability can be attributed to the North Atlantic Oscillation (NAO). The NAO is described in terms of shifts in sea level pressure between the polar and subtropical North Atlantic. The NAO index is a measure of pressure differences between Iceland and the Azores. A positive NAO leads to increased westerlies across the NA and cools the surface of the subpolar NA, whereas a negative NAO leads to weakened westerlies. Several studies, e.g. *Robson et al.* (2012); *Zhai and Sheldon (2012)*; *Bersch et al. (2007)*; *Eden and Willebrand (2001)*, investigated the oceanic response to the NAO and found immediate and delayed responses that manifest themselves in gyre circulation anomalies and heat transport changes associated with changes in wind-stress curl and changes in wind-stress.

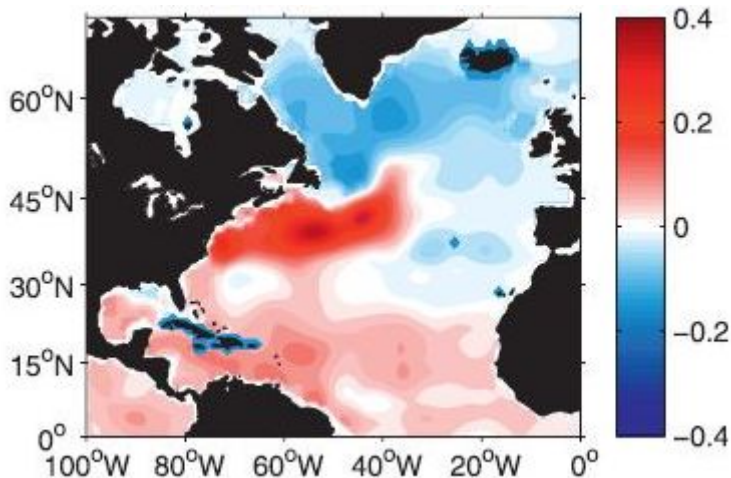


Fig. 6: Ocean heat content change between the periods 1955-1970 and 1980-1995 in the North Atlantic in the upper 0-700 m in 10^{20} J, from *Zhai and Sheldon (2012)*. The North Atlantic did not warm uniformly.

Before comparing estimates of the HC changes, it is important to mention that multi-year and seasonal variability of HC can be orders of magnitude larger on regional scales than on global scales (*Lyman*, 2012).

1.3 Current system and water masses in the study area

Heat in the ocean is advected by currents. The current system within the study area is depicted in Fig 7. The AX 3 section is located along the subpolar front, the area where the subtropical and subpolar gyres interact and strong temperature gradients are found. The waters on the polar side of this front are cold, fresh and ventilated, whereas the waters on the subtropical side are warm and salty. Along this subpolar front subduction occurs. The anticyclonic subtropical gyre in the North Atlantic has a strong and narrow western boundary current, namely the Gulf Stream (GS) that extends to the North Atlantic Current (NAC) east of the Grand Banks, Newfoundland. At Flemish Cap the NAC separates from the boundary and travels eastward as a free zonal jet transporting warm and salty water. Along its propagation path it splits into multiple branches. The southward branches become part of the subtropical gyre circulation and the northward branches feed into the Labrador, Irminger and Norwegian Seas as part of the subpolar gyre circulation. The northward flowing water of the NAC becomes source of dense waters which are formed in the Nordic Seas and the Labrador Sea. The heat transport into these regions may influence the formation processes of deep water masses within these regions.

The Labrador Current is the western boundary current of the subpolar gyre. From the Labrador Sea it continues southward to the regions of Newfoundland. After passing Flemish Pass the current partly recirculates into the NAC and partly continues westward on the shelf as a shallow current.

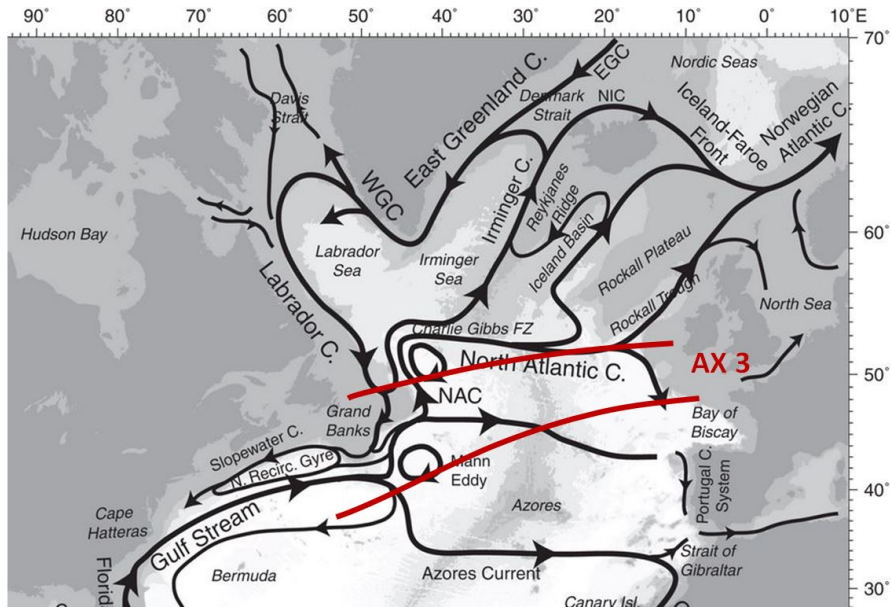


Fig. 7: Map showing the location of the AX 3 transect and the main current system.
(underlying map from Talley et al. (2011))

1.4 Aim and structure of this study

To analyse and understand the regional changes and spatial patterns of the HC change is important.

Related processes like ocean-atmosphere interactions and sea level rise have an effect at regional scales. The aim of this study is to investigate the temporal evolution and variability of the upper oceanic heat content on a regional scale along a section across the Atlantic basin. The main questions, that this study

seeks to answer, are:

- How is the HC evolving temporally?
- How is horizontal and vertical distribution of the HC?
- Are there trends (warming or cooling signals) detectable?
- How do the results compare to former estimates?

- May the results be linked to physical processes?

The next chapter describes the type and distribution of the data. The characteristics of the instruments, their functionality and their bias are outlined. Different methods to calculate the HC are introduced and the application and testing of two
5 gridding methods are described. In the third chapter the results are presented, which will be summarised and discussed in chapter four.

2 Data and Methods

The XBT data used in this study were collected within the Ship of Opportunity Program (SOOP) and provided by the Bundesamt für Seeschifffahrt und Hydrographie (BSH) Hamburg which performed a quality control. The XBTs were mainly
5 of type Deep Blue and Fast Deep and launched mostly from volunteer vessels.

Transects within the dataset that were not located in a comparable area were not taken into account. For the AX 3 section 9789 stations of 186 cruises covering the period 1988-2012 were used for the analysis (see Fig 8).

Annual and monthly climatological temperature data of the the World Ocean
10 Database (WOD09) in a 1° grid are used for the reference reference values in order to calculate the HC and to remove the seasonal signal from the data.

As the XBT data were sofar unpublished they allow for an estimate of the HC, which is independent from former studies.

2.1 Study area

15 Most of the formerly mentioned studies estimated the global ocean heat content combining observational datasets derived with various methods. In this study the focus is on a regional scale and the temperature measurements are taken solely by XBTs.

Repeated sections across the ocean help to investigate changes of upper ocean
20 and intermediate watermass properties and to obtain long and continuous time series at approximately similar locations in order to seperate temporal from spatial variability.

The AX 3 line crosses the North Atlantic between Europe and Newfoundland. Measurements across this line were carried out approx. four times a year between
25 1988-2012.

The transects of the ships are not exactly repeated due to weather conditions and currents. So the measurements experience a seasonal bias and are spread over a broad band of up to several hundred nautical miles width (see Fig 8 and Fig 9). Therefore it is not possible to analyse the measurements as if they would be distributed along a single section. In order to investigate the temporal evolution of the HC along a single section, a reference section was chosen (see Fig. 10) which represents a mean track closest to the largest amount of data. This will be used for the interpolation of the observed data in order to obtain time-series of HC.

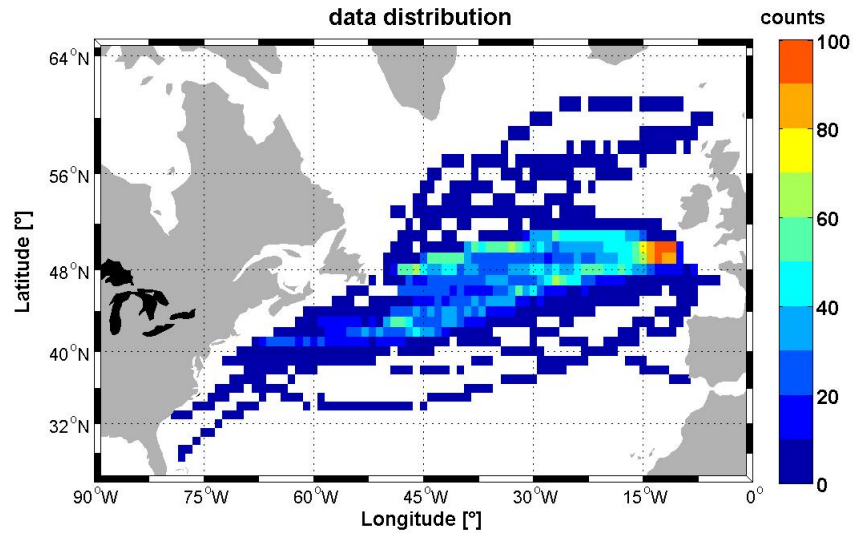


Fig. 8: Map showing the spatial distribution of the AX 3 data for the period 1988-2012. The shipping tracks do not follow a single line but may spread several hundred nautical miles

As can bee seen in Figure 9 the majority of data is confined to the region between -50° to -10° West and 40° to 50° North. The HC estimates are therefore calculated

within this area. From 2003 less data are available, with no data in 2009.

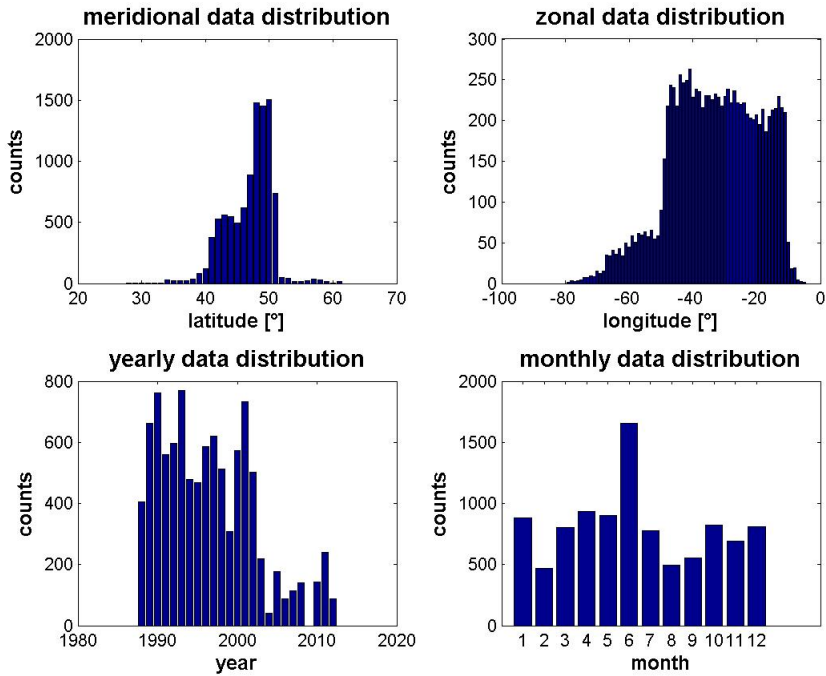


Fig. 9: Histograms of the spatial and temporal distribution of the AX 3 data

2.2 eXpandableBathyThermograph (XBT)

XBTs are widely used to observe the vertical thermal structure of the upper ocean. Until the Argo array was introduced they contributed 50% to the global ocean thermal observations (Goni *et al.*, 2010). The probes were initially developed for the Navy as a cost effective, robust and easy to handle instrument to estimate sound speed profiles (Scott, 2009). Most of the XBTs were manufactured by Sippican Corporation and Tsurumi Seiki Co. (TSK). The Deep Blue probes were introduced in the 1970s and designed to sample to a depth of 750 m and may be launched from ships traveling as fast as 20 knots. The temperature is measured with a thermistor which is placed in the nose of the probe. The accuracy of the temperature is within

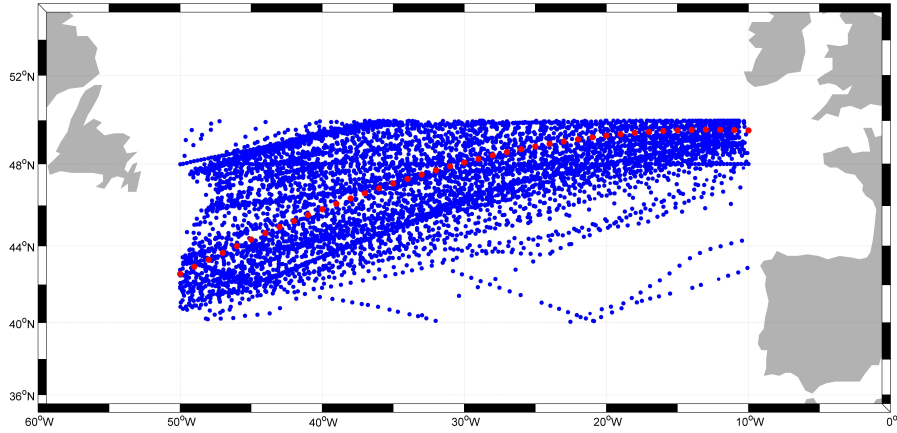


Fig. 10: Positions of stations (blue) and reference section (red)

$\pm 0.15^\circ\text{C}$ (Molinari, 2011). Depth is not measured directly but inferred from a fall rate equation (FRE) with empirically determined coefficients a and b in the form of:

$$Z(t) = at - bt^2 \quad (3)$$

Z is the depth at time t . The first term of the equation is related to the hydrodynamic characteristics of the probe in the water and the second term is related to the loss of mass of the probe as the wire is unspooling.

The depth uncertainty lies within $\pm 2\%$ or $\pm 5\text{m}$ depending on which value is greater (Molinari, 2011).

2.2.1 Probe design and operation

The probe main components are a thermistor, a copper wire that connects the thermistor circuit to the on-board record device and a hydrodynamical shaped



Fig. 11: The components of a eXpandable BathyThermograph (XBT) as described in section 2.2.1.

body. The body consists of a heavy metal nose cone which is attached to a hollow plastic tail. To make sure the probe sinks vertical the tail is equipped with fins. The thermistor is placed in the nose of the body. The wire is wound up in a coil within its shell, which remains on-board after launch, and a coil within the body of the probe. The data is collected until the wire breaks and the probe is lost. The probe is inserted into the launcher unit which fires automatically or by hand.

2.2.2 Bias

Biases in temperature measurements may result in erroneous estimates of HC variability. Uncertainties in the determination of XBT depth are the most important error source (Goni *et al.*, 2010). Additionally errors attributed to a temperature bias and to air-water transition during the launch of the probe may also be effective. A big general problem to handle historical XBT datasets is the lack of metadata, e.g. probe type, leading to additional uncertainty.

Since the 1970s systematic errors were identified (Goni *et al.*, 2010). Errors may arise from differences in the physical characteristics of the probes, differences in acquisition systems, transient effects in the near surface layer, launching conditions

and inaccuracies of the fall rate equations. The weight and changes of the probe , e.g. due to density of the wire, can influence the fall rate. It was found that the probes need some time to adjust to the temperature of the surrounding water and that the difference between storage room and water temperature might effect 5 measurements close to the surface (*Gouretski and Reseghetti*, 2010). Launch height, angle of impact, ship speed and waves may influence the dynamics of the probe and lead to a surface offset (*Goni et al.*, 2010; *Gouretski and Reseghetti*, 2010). The fall rate also varies with water temperature due to the effect of viscosity, i.e. the colder the water the slower the fall rate.

10 In former studies it was figured out that the coefficients in the fall rate equation provided by the manufacturer were not correct. Simultaneous CTD and XBT casts where compared and a small positive bias above the thermocline and a larger negative bias at greater depths were found (*Goni et al.*, 2010). There have been approaches to correct the biases that differ in methodology (e.g.*Hanawa et al.* 15 (1995); *Wijffels et al.* (2008); *Ishii and Kimoto* (2009); *Gouretski and Reseghetti* (2010)). Prominent examples of the effect of this instrumental bias is the artificial signal of warming in the ocean around 1975-1985 in the global ocean HC time series within 700 m depth in the study of *Levitus et al.* (2005). This signal disappears after correction of the XBT data, as well as the cooling signal reported in *Lyman* 20 *et al.* (2006) which appeared to be an artifact that results from combined XBT and ARGO instrument biases (*Willis et al.*, 2007, 2008).

Hanawa et al. (1995) found that the equation underestimated the actual fall rate: the probe is placed at shallower than its true depth thus measuring a lower than the actual temperature at a given depth. Uncorrected profiles gain a cold bias. *Hanawa et al.* (1995) compared XBT, CTD and bottle profiles taken at the same time and location. He determined new coefficients for the fall rate equation and provided a simplified correction scheme to obtain the corrected depth by multiplying a

stretching factor to depths derived from the original FRE:

$$Z = 1.0336 \cdot Z_{XBT} \quad (4)$$

Sippican replaced their coefficients for the fall rate equation with those derived by Hanawa in the mid 90s.

- ⁵ While studies by *Hanawa et al.* (1995); *Wijffels et al.* (2008); *Ishii and Kimoto* (2009) focused only on the depth bias, *Gouretski and Koltermann* (2007) also identified a time varying positive temperature bias of the probes by comparing climatologies derived from XBT and CTD/bottle observations.
- ¹⁰ *Gouretski and Reseghetti* (2010) showed that using the same correction factor for all depths does not eliminate the total temperature bias over the whole water column effectively. Applying a constant correction factor or time varying factor increases the total bias compared to the manufacturers FRE. Furthermore they showed that the time-dependent bias may be explained as a combination of temperature bias attributed to a systematic depth error and of a pure thermal bias. They suggest a correction scheme that accounts for a depth independent, time variable temperature bias and for a depth-variable, time independent depth correction according to shallow and deep XBT types to eliminate the total temperature bias.
- ¹⁵ By using GEBCO digital bathymetry recent studies by *Gouretski et al.* (2012) confirmed these findings.
- ²⁰ In this study the correction scheme suggested by *Gouretski and Reseghetti* (2010) is used. XBTs of type Deep Blue were corrected using monthly varying thermal bias corrections and depth corrections that vary monthly and with depth. For some years, the dataset included depths that were calculated form the FRE with corrected coefficients suggested by Hanawa. In that case depths were calculated back to the Sippican values before applying the correction (see eq. 5). For the

XBTs of type Fast Deep two different FRE coefficients appear in the dataset. In 2009, LM Sippican confirmed $a=6.390 \text{ ms}^{-1}$ and $b=-0.00182 \text{ ms}^{-2}$ as right values for FD (Reseghetti, pers. comm.). Depths of Fast Deep XBTs with the wrong coefficients were corrected to the right value. No further corrections were applied to the Fast Deep XBTs. An example of a corrected DB temperature profile is shown in Fig. 12.

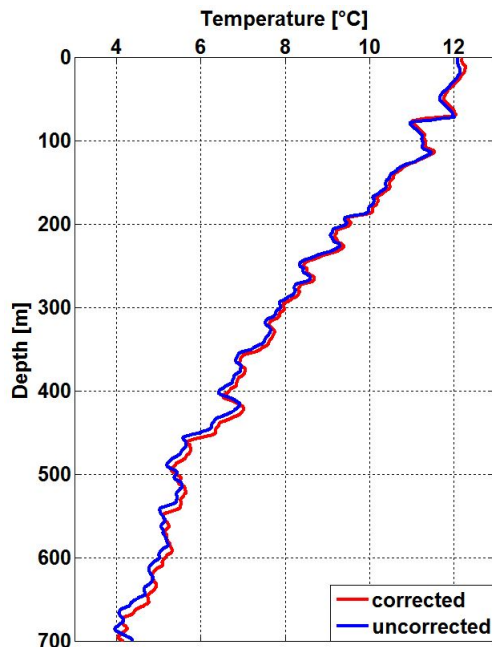


Fig. 12: Temperature profile taken by XBT of type Deep Blue before (blue) and after applying the bias correction

2.3 Calculation of Heat content

2.3.1 Heat content relative to a fixed depth

The classical approach to calculate the HC of a water column is done by integrating the difference between measured temperature and a reference temperature over a fixed depth level multiplied by the heat capacity and density (eq. 2). If one is not

interested in anomalies the reference values may be set to zero otherwise a mean state, e.g. obtained from a climatology, may be chosen. Due to dynamical processes, e.g. mesoscale eddies and internal waves, the position of temperature interfaces may be displaced and influence the HC estimates. To quantify this influence and 5 to describe the reasons for changes in HC another method is more useful.

2.3.2 Heat content relative to a fixed isotherm

Palmer et al. (2007) introduced a new method to calculate oceanic HC by integrating the difference between measured and reference temperature above the depth of a fixed isotherm. Their method, has the advantage that relative contributions of 10 advection and air-sea fluxes to changes in HC can be isolated. The changes of depth of the isotherm can be related to oceanic advection processes leading to vertical displacement of the isosurface but no gain or loss of heat. The temperature changes above a reference isotherm may be attributed to changes in air-sea heat fluxes leading to warming or cooling of the water column (see Fig 13).

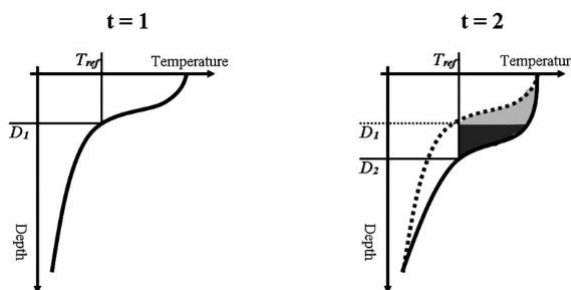


Fig. 13: Scheme of temperature profiles taken at different times. The HC may change due to heat input that raises the column-mean temperature above the isotherm (light grey area) and heat input due to deepening of the isotherm (dark grey area) .

15 Fig. 12, adopted from *Palmer and Haines (2009)*, illustrates these separate contributions From temperature profiles taken at the same location at different

times the heat input due to the deepening of the isotherm may be separated from the heat input which is required to raise the mean temperature of the column. Eq. 2 may be rewritten as

$$HC = c_p \rho_0 h (T_m - T_{ref}) \quad (5)$$

where T_m is the mean temperature above the depth of the fixed isotherm h

$$T_m = \frac{1}{h} \int_{-h}^0 T dz \quad (6)$$

- ⁵ The HC, the depth of the isosurface and the mean temperature may be split up into a time constant and a time varying part:

$$HC = \overline{HC} + HC'; h = \bar{h} + h'; T_m = \overline{T_m} + T'_m$$

Substituting this into Eq. 6 and omitting the $h'T'$ term, as it this is a product of variations and expected to be small, leads to

$$HC' \cong c_p \rho_0 h' (\overline{T_m} - T_{ref}) + c_p \rho_0 \bar{h} T'_m \quad (7)$$

- ¹⁰ The first term of eq. 8 is related to the displacement of the isotherm and therefore to dynamical processes, whereas the second term to changes in temperature due to air-sea heat fluxes.

2.4 Gridding

- The bias corrected data were interpolated linearly onto 1 m depth levels in order to obtain a consistent vertical resolution.

As the profiles are distributed irregularly in space as well, interpolation onto a regular grid and a reference section is necessary in order to create comparable estimates of HC. Two methods of interpolation were applied and compared to each other.

2.4.1 Barnes interpolation scheme

The Barnes scheme is an objective analysis which applies a Gaussian function where stations are weighted according to their distance from the gridpoint (see Fig. 14). Stations closest to the gridpoint contribute most to the overall value.

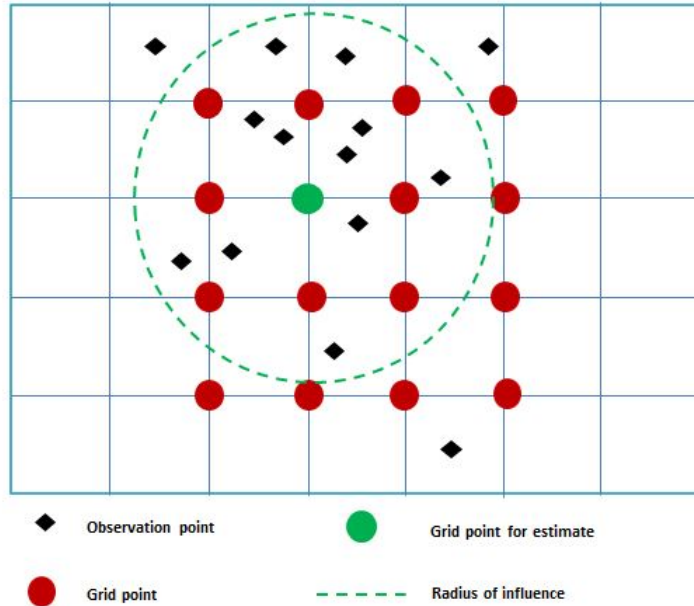


Fig. 14: Principle of the interpolation from observation locations onto a gridded field as applied in the Barnes scheme. Contributions of observations to the value on the grid point are weighted according to their distance from it. Observations outside the radius of influence are excluded.

- 5 The estimated values on the grid points are weighted averages of the surrounding stations which cause a smoothing of the field. After calculating the distance d between gridpoint and observation the weights W_i are calculated as:

$$W_i = e^{-\frac{d_i^2}{R^2}} \quad (8)$$

R is the radius of influence and operates as smoothing length scale, depending on the spatial distribution of observations and the scales of interest. Stations outside

this radius have no contribution to the total value of a grid point. For a first guess a value Z_g is estimated at each grid point g from the surrounding observations O :

$$Z_g = \frac{\sum O_i W_i}{\sum W_i} \quad (9)$$

In the next step a successive correction scheme is applied,, where the values on the grid are interpolated back to the points of observation. The difference between the
5 interpolated (Z_i) to the original value (O_i) is used as correction of the first guess value:

$$Z'_g = Z_g + \frac{\sum W'_i (O_i - Z_i)}{\sum W'_i} \quad (10)$$

with

$$W'_i = e^{-\frac{d_i^2}{(\gamma R)^2}} \quad (11)$$

During the correction passes the values on the grid are averaged and weighted values of the surrounding stations and therefore smoothed estimates. The degree
10 of smoothing is controlled by the smoothing parameter γ in eq. 11.

2.4.2 DIVA scheme

The second method is a data interpolating variational analysis (DIVA) which is designed to interpolate irregularly spaced data to desired locations. It was developed by the department of GeoHydrodynamics and Environment Research(GHER) at the
15 University of Liege. A detailed description of this method is given in *Troupin et al.* (2010, 2012). Here, only the general concept is described briefly. The idea behind this method is to estimate a field φ which is close to the data and also smoothed so that spatial variations are not too large. It is based on the minimisation of a cost function of the form:

$$J|\varphi| = \sum_{i=1}^N \mu_i |d_i - \varphi(x_i, y_i)|^2 + \|\varphi - \varphi_b\| \quad (12)$$

The first right-hand-side term of this equation denotes the difference between the analysed field and the observation (d_i). The weight μ_i is related to the signal-to-noise ratio (SNR) and the correlation length scale L :

$$\mu = SNR \frac{4\pi}{L^2} \quad (13)$$

The SNR gives an indication of the confidence the analyst has in the dataset
⁵ and of the strength of the signal compared to the noise of the data. Here the noise is not understood as caused by instrumental errors solely but also by the variability of the observations induced by subgrid processes, e.g. mesoscale eddies or internal waves. L is the typical scale of processes that are characteristic of the considered problem and determines the influence region of the data. The second
¹⁰ right-hand-side term in eq.(12) is a constraint to variability of the estimated field and can be understood as a measure of how strong the field varies. The $\| \|$ operator denotes an integral operation over the domain. The cost function J is solved with a finite element method. The DIVA interpolation is applied using the MATLAB version of this software which was downloaded from the GHER webpage
¹⁵ (<http://modb.oce.ulg.ac.be/mediawiki/index.php/DIVA>). During the analysis the background field φ_b represented by the data mean is subtracted and later added again, which means that interpolation is done with anomalies. The background field serves as a first guess of the reconstructed field. The analysis also delivers a relative error estimate which is scaled locally by the local variance.

²⁰ 2.4.3 Application and performance of interpolation

As the results of the interpolation methods depend on the distribution of the observations and the choice of the smoothing length scales and signal-to-noise ratio, those parameters have to be chosen reasonably. Here the choice of these parameters is made after applying tests of the methods on a known field in respect to the

data distribution. The reference field for these tests was chosen to be close to the expected observations in terms of spatial characteristics and magnitudes of the values. Therefore the WOD09 climatology (see Fig. 15) was used to calculate the "true" values of the HC along the reference section. The two interpolation
 5 methods were applied to a subset of data points and the interpolated estimates of HC along the reference section were compared to the known reference values. The best setting of parameters was found when the difference was smallest. In this way the setting for the parameters could be obtained according to the distribution of data points within a year, and then be applied during the analysis of the observed
 10 HC. An example of this procedure is illustrated for the year 1990. Fig. 16 shows the climatological HC values at the location of observation for this year. The "true" value of the HC along the reference section is plotted in Fig. 17. The deviations of the interpolated values from the "true" values along the reference section are depicted in Fig. 18.

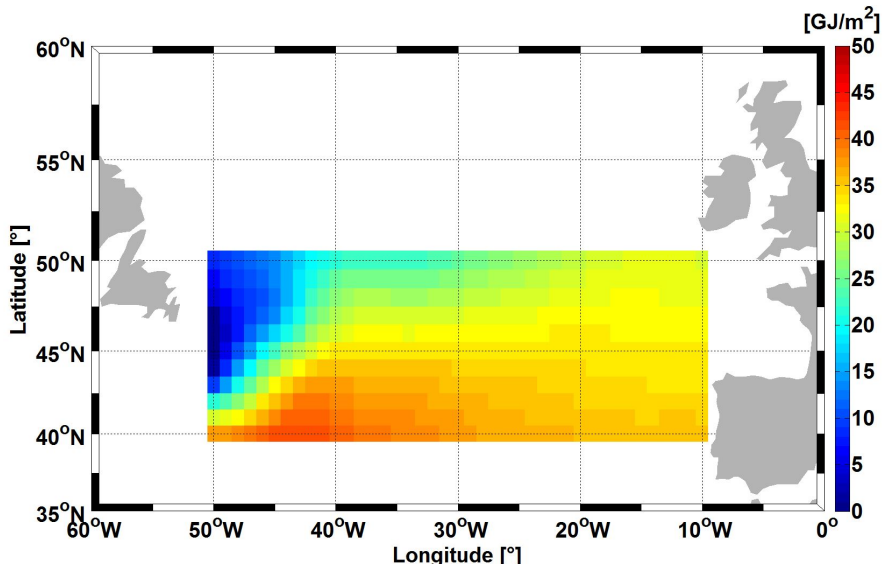


Fig. 15: Reference field of HC within the analysed domain on the basis of WOD09 climatological data

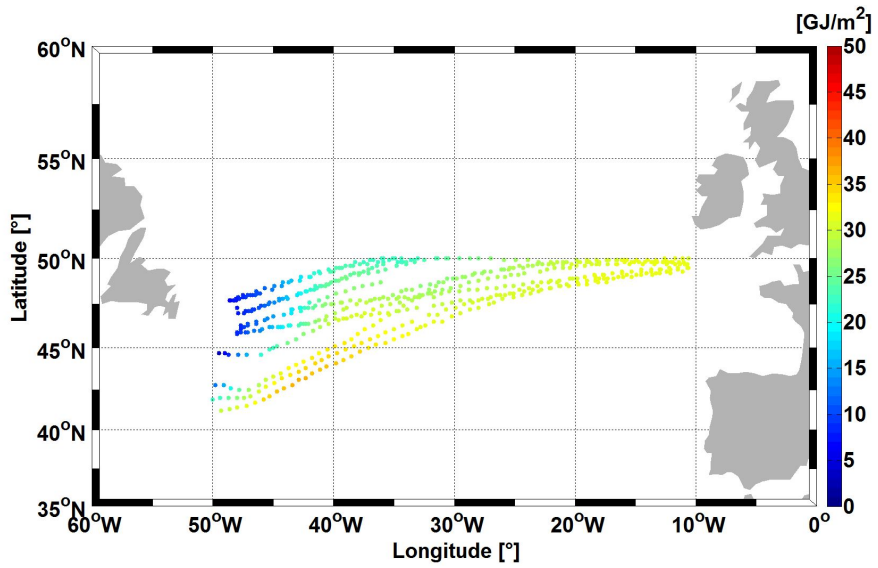


Fig. 16: Climatological reference values at observation points for the year 1990

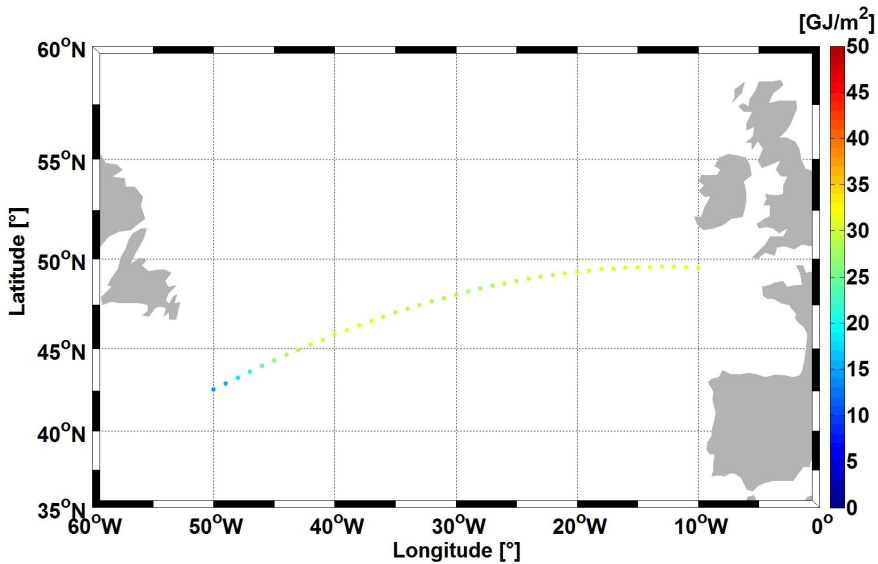


Fig. 17: Climatological reference values at the reference section

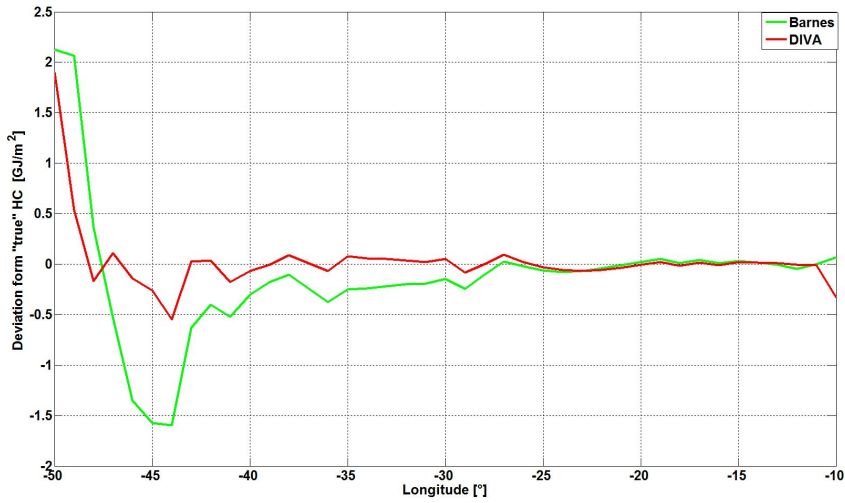


Fig. 18: Deviation of interpolated HC estimates from "true" value: barnes estimate (green), DIVA estimate (red)

This procedure was done for every year respectively and by minimizing the deviation from the "true" HC optimal parameters were estimated that fit best for all years together in order to have a single consistent setting for the further analysis. For DIVA the SNR was set to 10. For both methods the length scale was
5 set to 4° in Y direction and 3° in X direction. Please note that the distance of 1° in the longitudinal direction is dependent of the latitude. The radius is therefore not isotropic as the length scale in X direction ranges between approx. 255 km (at 40° N) and 213 km (at 50° N). The chosen length scales are a compromise in order
10 to have a sufficient amount of datapoints for a reasonable interpolation and at the same time smoothing out the small-scale features which are not of interest. From section plots it can be seen that eddy structures have typical radii in the order of 100-200 km. Therefore it is expected that eddies will not be filtered out completely and their influence on HC estimates has to be considered in the further analysis.
15 In order to investigate the performance of the interpolation methods time series of the climatological HC along the reference section were calculated.

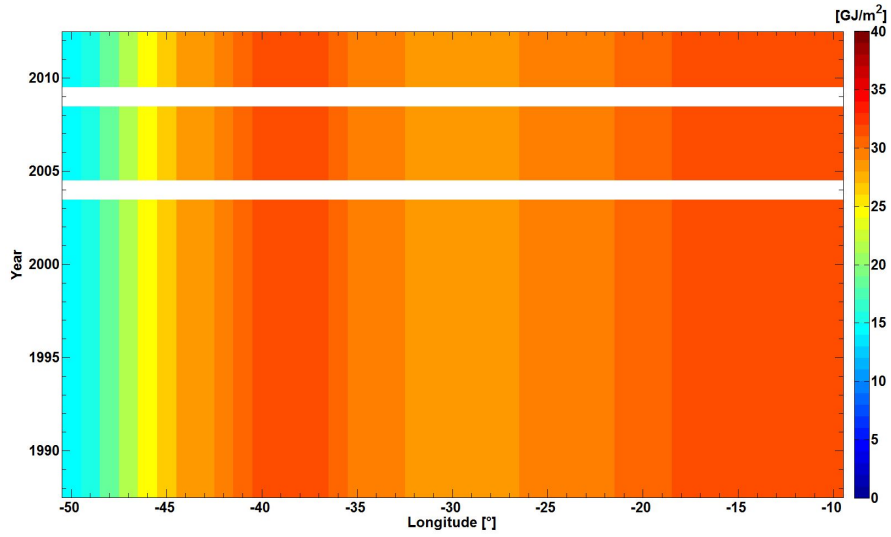


Fig. 19: Climatological HC values on reference section as function of longitude and time.

Fig. 19 depicts a Hovmoeller plot of the "true" climatological HC values as a function of longitude and time. At a given longitude the values are expected to be constant over time. Fig. 20 and 21 show the results after applying the DIVA and Barnes methods, the deviations from the "true" estimates are plotted in Fig. 22 and 23.

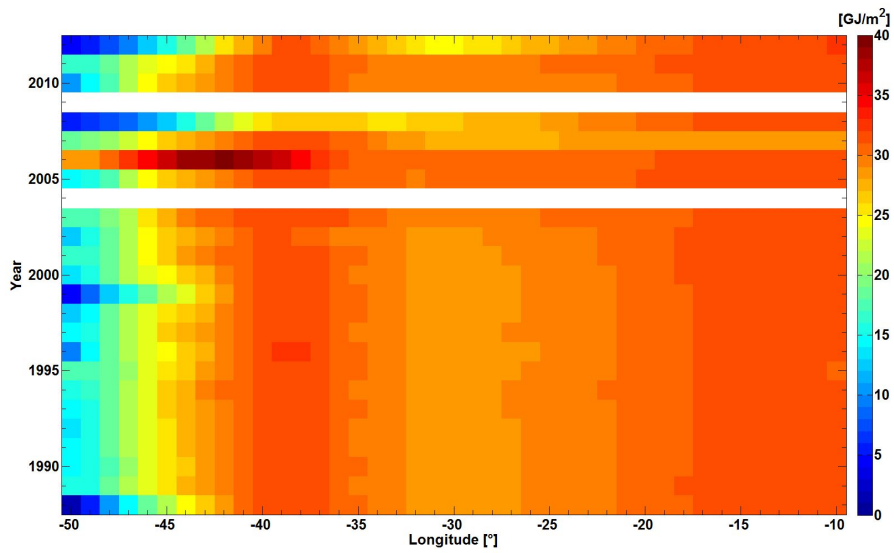


Fig. 20: Climatological HC values on the reference section as function of longitude and time after applying Barnes interpolation scheme.

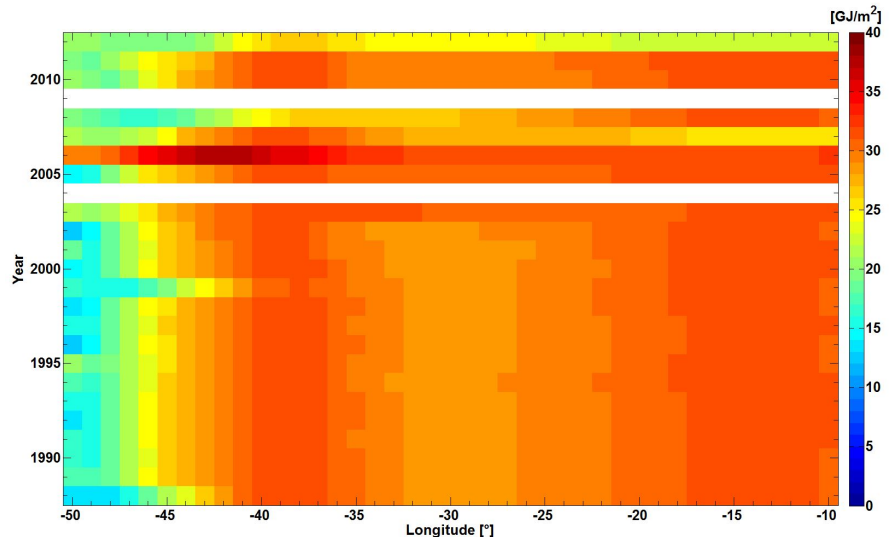


Fig. 21: Climatological HC values on reference section as function of longitude and time after applying DIVA interpolation scheme.

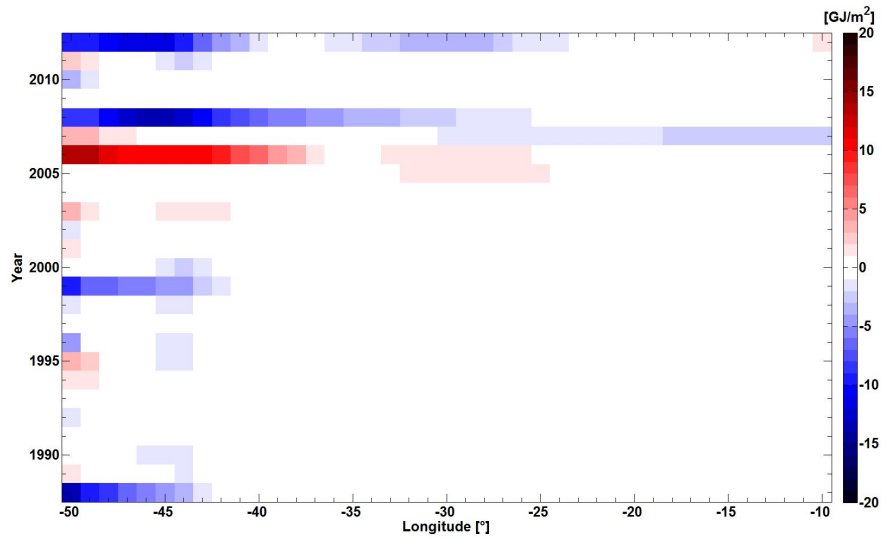


Fig. 22: Deviation of HC from "true" climatological values on reference section as function of longitude and time after applying Barnes interpolation scheme.

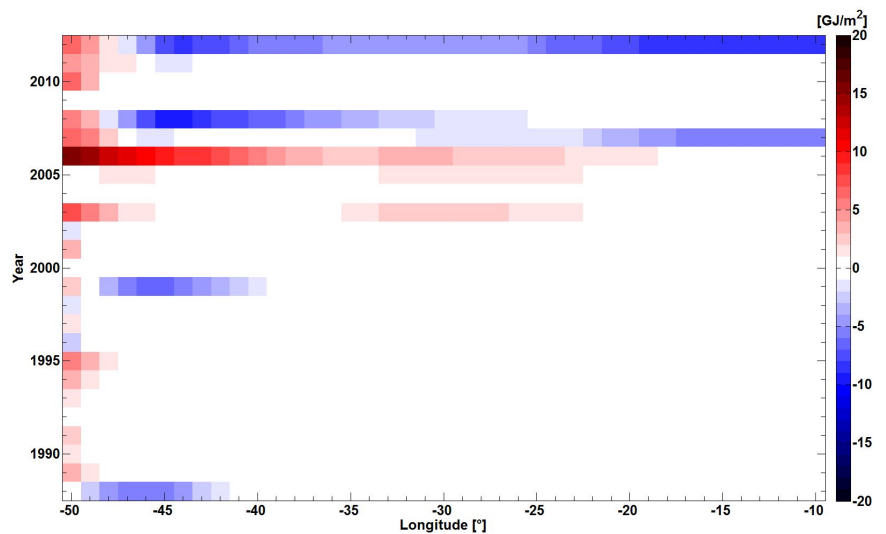


Fig. 23: Deviation of HC from "true" climatological values on reference section as function of longitude and time after applying DIVA interpolation scheme.

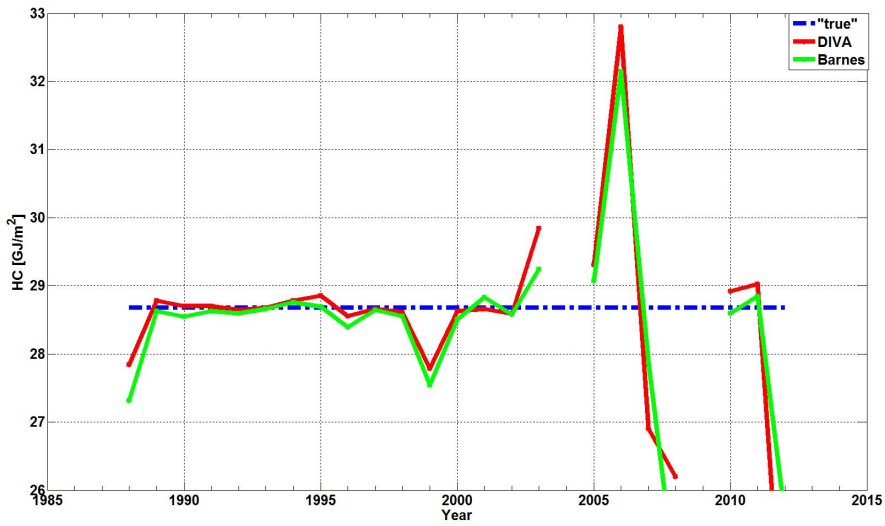


Fig. 24: Time series of mean climatological HC of reference section (50° - 10° W) after applying DIVA (red) and Barnes (green) interpolation schemes.

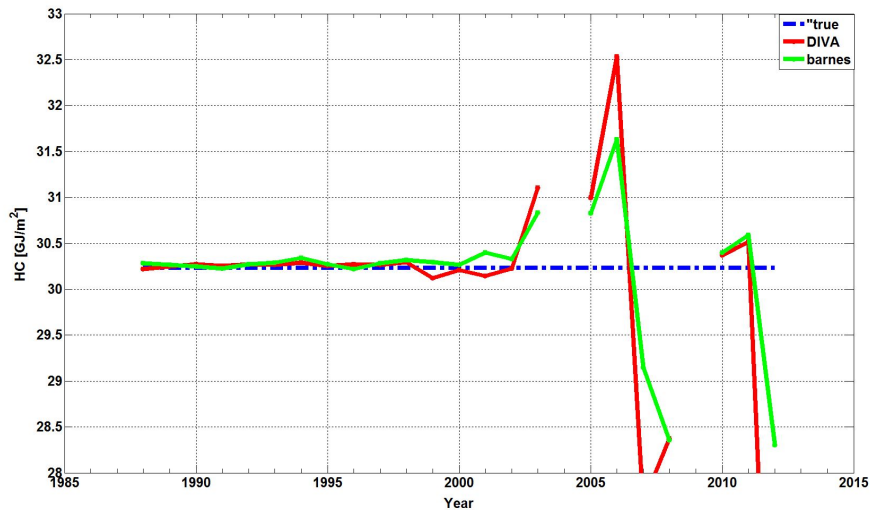


Fig. 25: Time series of mean climatological HC of shortened reference section (41° - 12° W) after applying DIVA (red) and Barnes (green) interpolation schemes.

The largest differences with amplitudes of up to 15 GJ/m^2 occur mainly in the westernmost part of the section, during 1988, 1999 and from 2003. Between 2005 and 2008 the deviations expand also to the eastern part. From Fig. 18 can be seen that also at eastern border small deviations occur. These features have
5 an important effect if one considers time series of mean HC of the section. In Fig. 24 the time series is depicted for the complete section whereas in Fig. 25 a shortened section, which reaches from 41° to 12° W and does not include the areas large interpolation errors, is shown. From this plots it can well be seen that the interpolation itself induces variability which is erroneous. The reasons for the poor
10 estimates, especially at the western border of the domain, are assumed to be due the lack of a sufficient amount of data points that are used for the interpolation. The fact that in this regions the gradients are strongest are also suggested to have an influence on the performance of the interpolation schemes. The smoothing may lead to estimates which deviate strongly from the "true" values. The comparison
15 of the full and shortened sections suggests to exclude the westernmost part of the section or at least consider it separately. Also the years after 2003 give very poor quality of estimates, which is assumed to be due to the sparse observations at these times. Both interpolation methods show similar results. After 1998 the estimates diverge but the DIVA method seems to give slightly better performance. Therefore
20 it is used for the further analysis.

3 Results

To remove the seasonal signal within the data climatology from WOD09 were used. Monthly climatological temperature offsets in respect to an annual climatological mean were corrected according to month, position and depth of the observations.

- 5 The DIVA interpolation scheme was used for interpolation onto the reference section with 1° intervals in zonal direction to produce time-series of HC and on a horizontal grid with a 0.1° resolution to produce horizontal maps. To calculate the HC, the heat capacity c_p was set to $4000 \frac{J}{kgK}$ and density ρ_0 to $1025 \frac{kg}{m^3}$

3.1 Temperature Section

- 10 Analysis of temperature profiles along the reference section reveals information about the vertical structure and evolution of the temperature field and anomalies. Exemplary Fig. 26 shows a section for year 1993 (other years are not shown) Compared to the climatological section, the warm water extends to much greater depths, especially in the western part of the section. The warming occurred along
15 the whole section in this year. Analysing all years, a strong temporal and spatial variability of the temperature field is found. 1989 only a weak warm anomaly in the western part is visible. One year later a cool anomaly is found covering the whole section and extending from the surface to 700 m. In 1991 warm anomalies are found in the west and cold anomalies in the western part of the section whereas
20 in 2003 cold anomalies are found in the west and warm anomalies in the east of 23° . For 1995 the strongest warm signal is found at the surface extending $36^\circ - 18^\circ$ W and a core of a warm anomaly between $36^\circ - 29^\circ$ W at depth between 300 and 700 m. A bowl of warm water is located in the western part of the section but differing in horizontal extension, position and temperature within the observed period. For
25 1990 it is not found east of 41° W but in 2000 it extends to approx. 34° W. The

position of this bowl is supposed to be associated with shifts of the subpolar front. In 1999 a strong temperature gradient is located at 40° W indicating the most intense eastward shift of the subpolar front within the observed period. In almost every year bowed isotherms indicate eddy-like structures that cause warm or cold anomalies that also vary in their intensity.

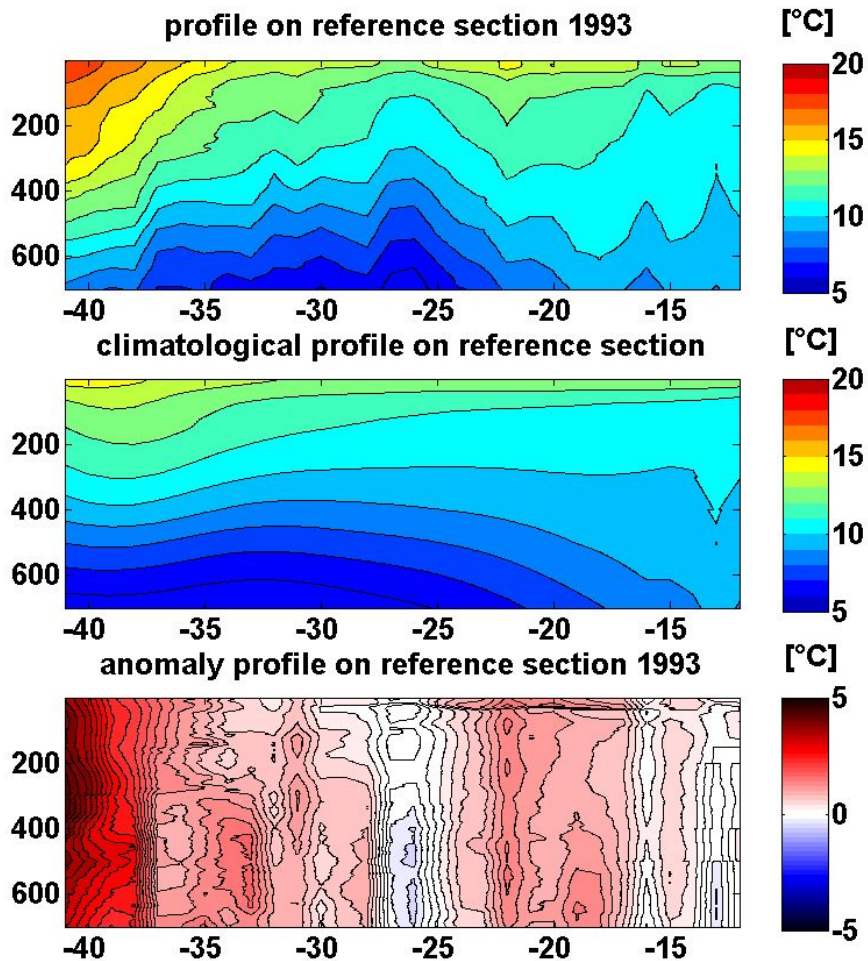


Fig. 26: Vertical temperature profiles along the reference section: measurements (upper panel), climatological values (middle panel), anomalies (lower panel)

3.2 HC time-series on the reference section

As described in chapter 2.4.3 in the westernmost part and in the easternmost part interpolation errors are largest and therefore the further analysis of HC timeseries is restricted to a shortened reference section (41° W to 12° W). Fig. 26 shows a time

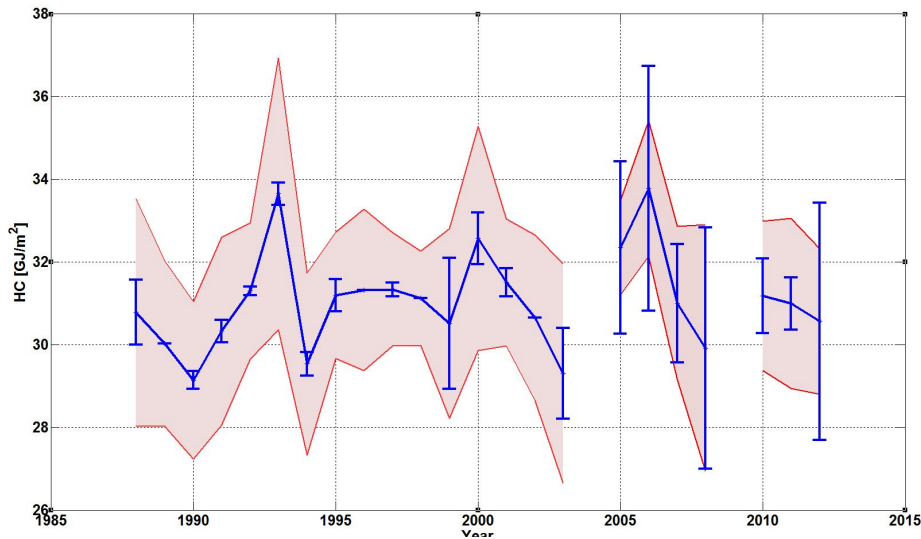


Fig. 27: Time series of the annual mean HC (0-700 m) along the reference section 41° W to 12° W. The blue errorbars indicate an estimate of the interpolation error. The red shaded area illustrates the standard deviation from the mean along the section.

- 5 series of the annual HC (0-700 m) averaged along this section. The blue errorbars are the maximal errors from the DIVA interpolation give a rough estimate of the quality of interpolation. These errors are large in 1999 and from 2005 due to the low amount of data. The red shaded area denote the spatial standard deviation along the section indicating the spatial variability of HC. The mean value of the
- 10 yearly HC and its temporal standard deviation is $30.9 \pm 1.2 \frac{GJ}{m^2}$. The temporal evolution shows a decrease in HC from 1998 to 1990 followed by a warming until 1993. The HC rapidly drops in 1994, raises again and then stays stable until 1999.

After a short warming period the HC decreases again until 2004. As the years from 2005 ongoing are supposed to be highly erroneous it is not possible to clearly detect a signal.

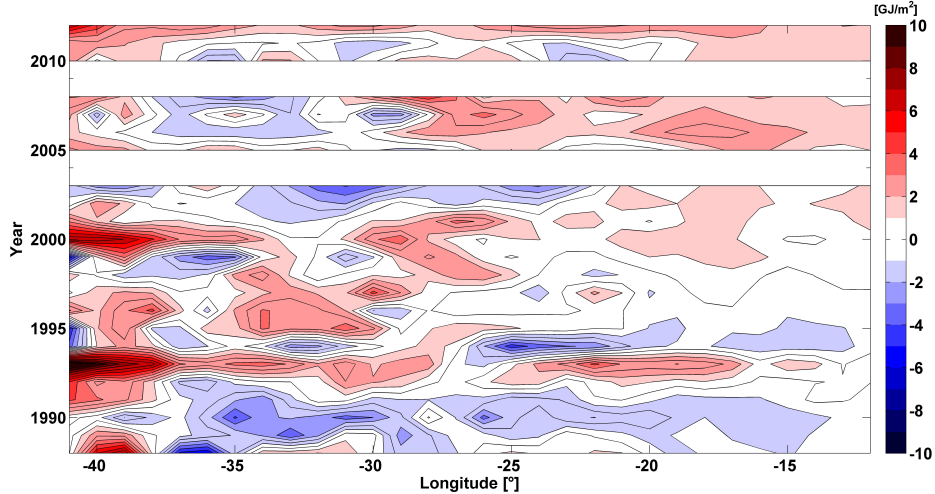


Fig. 28: Hovmöller plot of annual HC anomaly (0-700 m) along the reference section

The Hovmöller plot of the HC anomalies in Fig. 27 shows the strongest signals located in the western part between 41° W to 30° W. In 1990 a cooling signal extends along the whole section and in 1993 a warm anomaly has its largest amplitude in the west but extends far to the east. For other years, e.g. 1996 where a strong warm anomaly can be found in the west but not in the eastern part of the section, the signal is distributed non-uniformly in space. Dominantly warm signals are found west of 30° W. At this position the NAC encounters the Mid Atlantic Ridge (MAR). The MAR is an obstacle for the current and crossings are confined to topographic fracture zones. Changes in pathways of the NAC may bring more warm water to the northeastern regions of the North Atlantic as found by Häkkinen and Rhines (2009). Consistent with their studies more warm anomalies are found in the east of the position of the MAR after 2001. Calculating the mean HC timeseries only for the part of the section east of the MAR (30° - 12° W), reveals

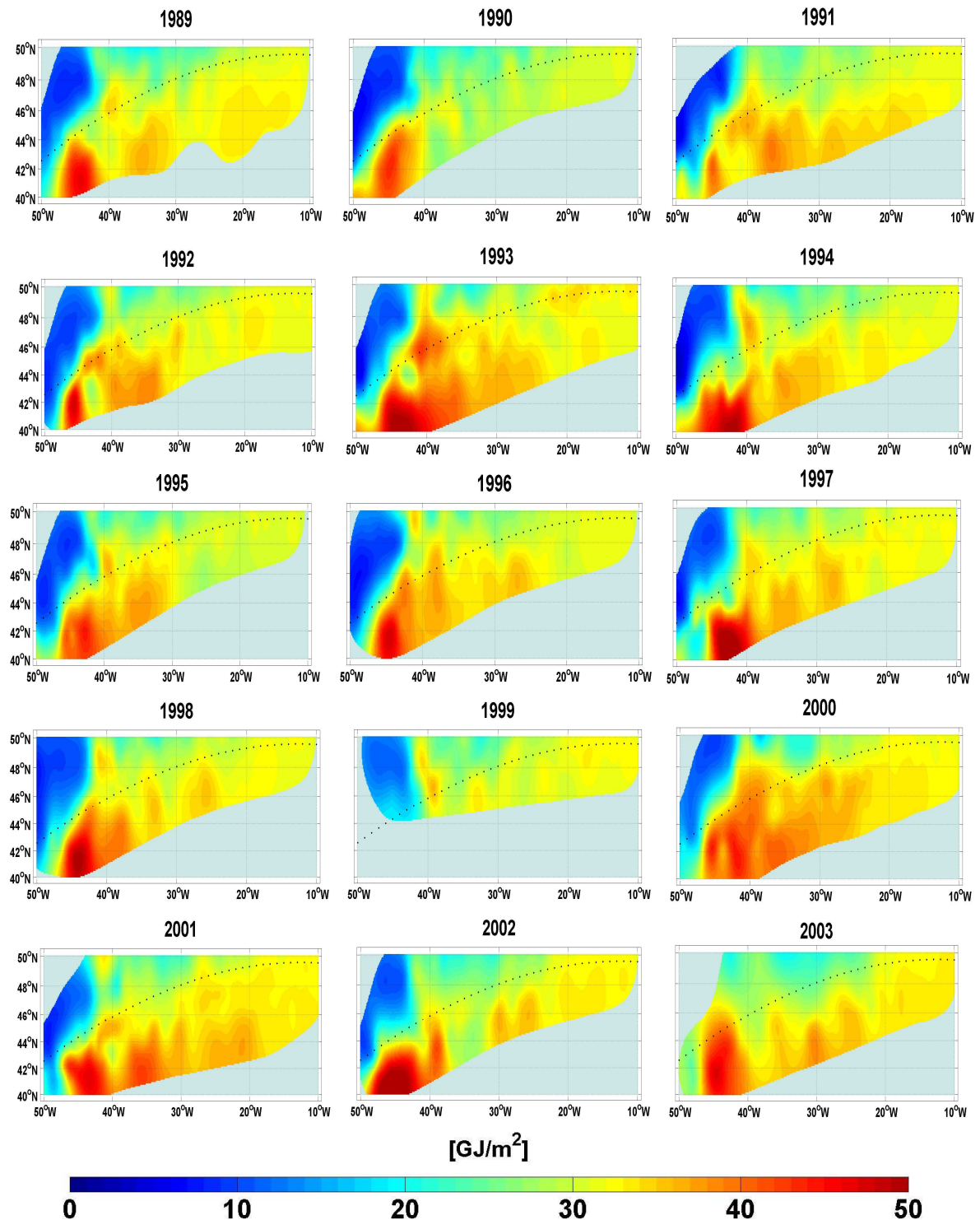
a continuous rise of HC from 1996 to 2001. Considering only the western part (41° - 30° W) within this period a decrease of HC is found beginning at 1997 with a minimum in 1999. Beside the spatial variability, it can also been seen that shifts between cold and warm anomalies occur within inter-annual timescales.

5 3.3 Horizontal maps

The positions of the XBT sections are not repeated exactly but may spread over several hundred nautical miles within one year. This fact is obstructive to produce time-series of HC along a single section. On the other hand it allows the construction of horizontal maps of HC estimates as shown in Fig. 28. The most striking feature
10 is the strong subpolar front, separating the cold water masses from the warm Atlantic water which is transported by the NAC. The strongest gradients occur at the distinct front east of Grand Banks where the southward Labrador Current transports cold water southward. The position of the subpolar front is not fixed but propagates in North-South and East-West direction. The reference section of
15 the XBT profiles is located on a transition zone and estimates of HC are strongly affected by the location of the front. In 1990 the front is not reaching far enough north to affect the section east of 41° W resulting in the HC minimum in this year. In 2000 the front can be found far more in the north at 48° to 50° N and along the whole section explaining the maximum in HC in these years. The position
20 of the front may differ strongly from year to year. These shifts of the front are associated with changes in circulation due to changes in atmospheric forcing (*Eden and Willebrand, 2001; Bersch et al., 2007*). In 1992 and 1995 a gradient in HC at 30° W is visible. This suggests some influence of the MAR on the pathway of the NAC and the transport of warm water downstream as described in the chapter 3.2.
25 In 1991 and especially after 2000 the warm water reaches farther north-east. Some eddy-like features are apparent characterized by some warm/ cold cores as well

as narrow bands of warm/ cold patches stretching in north-south direction. Such mesoscale dynamical phenomena as also seen on the vertical plots may influence the HC estimates if not filtered out. In 1993 such warm core structures contribute to the maximum of HC in this year.

Fig. 29: Yearly Maps of HC (0-700) in GJ/m^2 and reference section (dotted line)



3.4 HC relative to fixed isotherm

In order to relate the variability of HC to its cause one has to distinguish whether those changes occur due to dynamical processes or due to air-sea heat fluxes. Therefore the approach of *Palmer and Haines* (2009) is applied. A detailed description of this method is given in chapter 2.3.2 The HC is calculated relative to a fixed isotherm. In this case the 11 ° isotherm is chosen as it is covered over the whole section through all years. Its mean depth is at 311 m. Following eq. 8 the part attributed to depth changes of the isotherm and those to temperature changes above the isotherm are calculated separately. For each year and each gridpoint along the reference section the difference in the depth of the isotherm and the difference of mean temperatures above isotherms were calculated. To compare the estimates the HC above 311 m was calculated additionally with the classical approach following eq. 2. Fig. 30 shows the time-series with the first part of eq. 7 (D-term, red), the second part (T-term, green), their sum (HC_{11° , blue), and the classical estimate (HC_{311m} , black). There is good agreement between the classical and the isothermal approach in the HC estimates. The contribution of the dynamical term to the total estimate clearly dominates in 1990. From then until 1993 both terms contribute almost equally while later on the changes in HC due to temperature changes appear to be the main contributor. As mentioned earlier the years after 2003 have to be seen with caution due to the lack of data. The fact that the time-series are very short, with only few data points due to the yearly averaging, restricts the statistical analysis if the focus is on trend estimates. This can be shown if one considers the HC time series from Fig. 30 for the first 16 years from 1988-2003, where the estimates are more reliable in terms of interpolation errors. If we calculate the mean of this time series and its 95% confidence interval following Eq 3.8.6 in *Emery and Thomson* (2004) we get $\overline{HC} = 0.35 \pm 0.30 \frac{GJ}{m^2}$. If

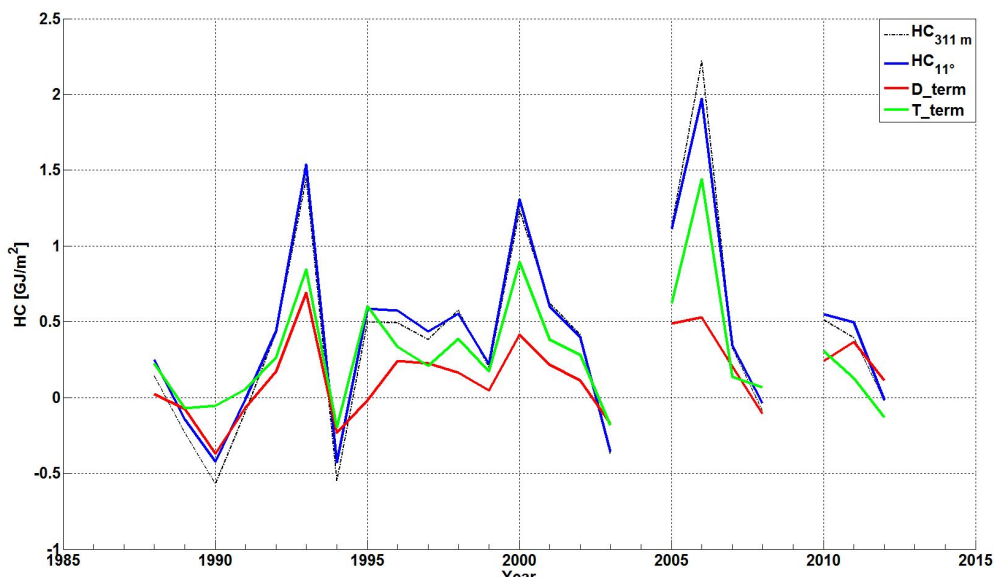


Fig. 30: Time-series of annual HC anomaly relative to 11° isotherm (blue), the dynamical contribution (D_{term} , red), the heat flux contribution (T_{term} ; green) calculated following eq. 7 and the HC above the mean depth of the isotherm (311 m) calculated following eq. 2

now a linear trend is estimated using a linear regression function of the form

$$\hat{y} = \beta_1 x + \beta_0 \quad (14)$$

,where β_1 is the slope and β_0 is the intercept, it can be seen in Fig. 31 that the trend line (black) lies within the confidence interval (green) of the mean (red).For this reason a trend can not be separated from noise within the mean estimates. Linear trends for the period 1988-2003 in Wm^{-2} and their standard errors are

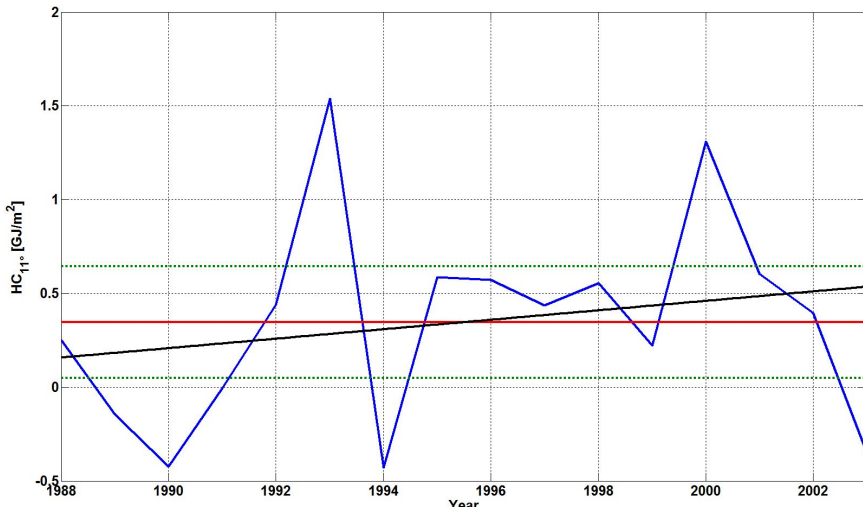


Fig. 31: Time-series of HC anomaly relative to 11° isotherm (blue), time mean (red) and its 95 % confidence limits (red). A regression line (black) is fitted to the data.

5

calculated for the HC (0-700 m), HC_{11° and its contributors D-term and T-term. To analyse spatial differences it is distinguished between the full section (41° W to 12° W) and 10° segments. The estimates are summarised in Table 1. For the whole section a positive trend is found for the different HC calculations. Considering
10 the single segments the western part shows a negative trend whereas the trends in middle and eastern part are positive. The largest increase in HC in the observed period is found in the eastern segment. Again it has to be noted that the errors

Longitude	HC (0-700m)	HC _{11°}	D_term	T_term
41° - 12° W	0.91±2.05	0.80±0.97	0.39±0.44	0.41±0.57
41° - 31° W	-1.45±3.51	-0.14±1.77	-0.29±0.71	0.14±1.14
31° - 21° W	0.65±2.18	0.95±0.86	0.46±0.44	0.50±0.46
21° - 12° W	3.26±1.23	1.54±0.54	0.98±0.40	0.56±0.22

Table 1: Linear trends and standard errors in Wm^{-2} of HC (0-700m), HC_{11°}, D_term and T_term for the period 1988-2003

of trends are large, mostly of the same magnitude or even larger as the trend estimate itself. This suggests that a linear fit of the time-series is very uncertain. The magnitude of the trends compare well to the trend of $0.72 Wm^{-2}$ calculated by *Palmer and Haines* (2009) for HC relative to the 14° isotherm in the North Atlantic for the period 1970-2000. They are larger than global ocean HC (0-700 m) trends of $0.27 Wm^{-2}$ calculated by *Levitus et al.* (2012) for the period 1955-2010.⁵

3.5 HC and NAO

As former studies found the variability in HC in the North Atlantic is related to the NAO (see chapter 1.2). To investigate if such a relationship is found, HC time-series are compared to the Hurrel NAO-winter index. To take into account a lagged response of HC changes to NAO changes a lag-lead analysis is performed. Fig. 32 depicts the correlation coefficients r for 16 y segments of the NAO index time-series for the period 1948-2012 which are shifted for 1 year and correlated with the HC (0-700) time-series for the period 1988-2003. The red dotted lines depict the 95% significance level and the green dotted lines the 90% significance levels. There are only a few significant correlations found at the 95% level. Interestingly the highest correlation is found at a lag of 7 years. This means the NAO would lag

the HC 7 years. Although it might not be impossible that the HC feeds back on the atmosphere and there for influences the NAO, this result is surprising. From former studies it would have been expected that the HC lags the NAO within 2-3 years (Eden and Willebrand, 2001; Visbeck *et al.*, 2003). In this analysis no significant correlation is found at this lags. As there is still a 5% chance the the significant correlations that were found may have occurred randomly, it is not clear whether this correlations are caused by to real physical processes.

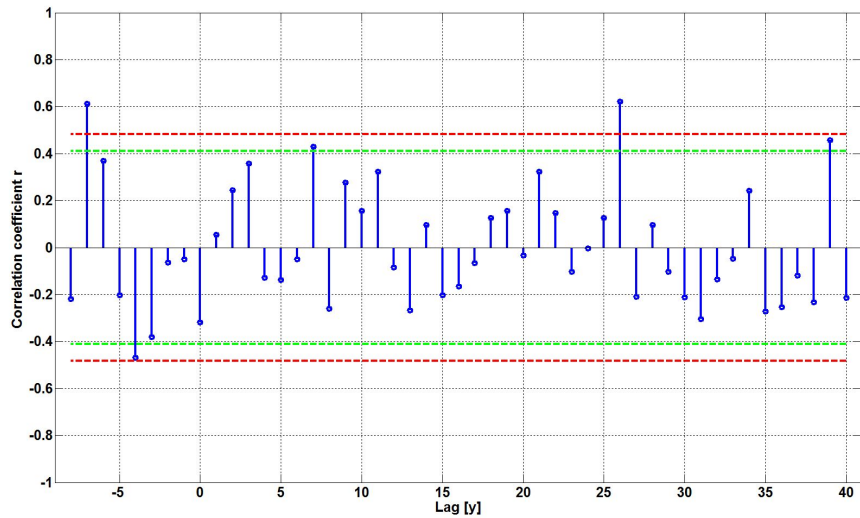


Fig. 32: Correlation coefficients from a lag-lead analysis. 16 y segments of the NAO winter index time-series for the period 1948-2012 were shifted in 1 y steps and correlated with the annual HC (0-700) time-series for the period 1988-2003. The red dotted line indicates the 95% significance level and the green dotted line indicates the 90% significance level.

4 Summary and Discussion

In this thesis a XBT dataset from repeated sections of the SOOP program across the North Atlantic between Great Britain and Newfoundland was analysed. Focus

of the analysis was the variability of HC over the period 1989-2012. The XBT data are known to suffer from temperature and depth biases. Therefore correction schemes following *Gouretski and Reseghetti* (2010) were applied. To remove the seasonal signal the date were corrected using monthly climatologies from the World Ocean Database 2009. In order to investigate the temporal evolution of HC by producing time-series, the data had to be interpolated onto a reference section as the transit lines of the ship routes differ in their position. A Barnes interpolation scheme and a interpolating variational analysis (DIVA) were applied and their performance tested. As it turned out, due to the spatial and temporal scattering of datapoints variability was induced to HC estimates resulting from interpolation errors solely. To reduce this source of errors the HC estimates were reduced to a yearly basis and to a shortened reference section located between 40° to 50° N and 41° to 12° W. Both interpolation schemes gave similar results and with slightly better performance of the DIVA method. This method was then used for further analysis. After 2003 the amount of data was reduced strongly resulting in large interpolation errors in the following years. Therefore these years are not considered in the following discussion. Time-series of mean HC (0-700) along the section show strong variability with cooling until 1990 followed by warming until 1993. Shortly after another HC minimum is reached in 1994 again followed by warming period and almost constant values between 1995 and 1998. In 2000 a maximum occurs followed by a cooling signal until 2003. It was shown that most of the variability is induced by signals in the western part of the section, with some exceptions where the warming signals extend over the whole length of the section. Comparison of the HC estimates with time-series of potential temperature of the upper 1000 m along a similar section from *Bersch et al.* (2007) for the periods 1993-2003 shows different results. Considering the western part from 27° to 12 ° W the temperature time-series (WEB in Fig. 12 of Bersch et al.) shows also an increase from 1994

until 2001, but without the drop in 1998 and a continued temperature rise until 2003.

The uneven positions of the individual transects can be used to produce horizontal maps in order to shed some light into the spatial structure of the HC distribution and causes of the variability within the time-series of the reference section. The most striking feature is the propagating position of the subpolar front. Also visible are eddy-like structures that may affect HC estimates as they transport anomalous cold or warm water. Vertical profiles depict that a bowl of warm water in the western part of the section is changing its position and warming/ cooling anomalies are visible over the whole depth of measurements. Again it can be seen that for some years the warming/cooling signals extend over the whole section and for other years there occur opposite signals between western and eastern part of the section. Mesoscale eddy structures that affect the HC estimates are identified due to the existence of bowed isotherms. In order to analyse the physical reasons for the variability another approach of calculating the HC was applied. Following *Palmer and Co-Authors* (2010), instead of integrating over a fixed depth level the HC was now calculated relative to a fixed isotherm. This method allows to isolate dynamical contributions of HC changes due to the change of depth of a reference isotherm from contributions of air-sea heat flux changes. A time-series of HC relative to the 11° C isotherm was calculated and then split up into its components. The dynamical contribution associated with circulation changes is dominating until 1990. From then until 1994 the heat flux term and the dynamical term have almost equal contributions. For the next years until 2003 the heat flux term is the dominant contributor to HC change relative to the 11° isotherm. This result is not consistent with the estimates of *Palmer and Co-Authors* (2010). Their results show a dominating contribution from depth changes over the investigated period, however they are covering a larger area of the North Atlantic and consider

the 14° isotherm. These results may be compared to heat flux estimates in the North Atlantic but this is beyond the scope of this thesis. The analysis of trends is restricted due to the shortness of the time-series. Regression coefficients are found to be not significant. As suggested in several publications the amount of heat transported in the region of interest is modulated by circulation changes and heat flux changes. These changes are connected to the strength of the sub-polar and subtropical gyres which is in turn are connected to atmospheric forcing expressed in changes of wind stress attributed to changes of NAO index. During a positive NAO the NAC is intensified and advects warmer subtropical water on its side and more colder water on its northern side resulting in strong meridional gradients and a sharpened SPF (Bersch et al.) Due to the shift of the NAO from positive to negative the transport of NAC decreased and the SPF moved northward.

A positive NAO leads to a cold northward shift of westerlies, the sub-polar gyre cools whereas the gulf stream warms. The SPG shifts westwards and is more intense.

Rolf Käse kindly provided me with HC estimates from a coupled model with NAO-like forcing (described in *Köller et al. (2010)*). Comparison with the HC time-series of this study indicates that variability within equivalent 16 y time spans of the much longer HC time-series (1000 y) along an equivalent section is part of the general variability. Rapid changes of HC in the 2-5 y spectral band are also found in the model. The variability of the long modeled time-series correlates strongly positively ($r=0.8$) with the intensity of the Gulf Stream agged by 3 years. The longer term variability of the HC time-series may be part of a mode corresponding to the Atlantic Multidecadal Oscillation (AMO), which is not resolved in our 16 year record.

Summarised, it can be noted the HC in the along the section across the Atlantic is highly variable in space and time. Due to the sparse observations a analysis of

the causes of the variability is restricted and statistical results considering trends and correlations can not be made with confidence.

To gain further insight into physical processes connected to changes of HC in the investigated region of the North Atlantic a extension of the time-series is necessary
5 and addition of data from other sources indispensable.

References

- Bersch, M., Yashayaev, I., and Koltermann, K. P. Recent changes of the thermohaline circulation in the subpolar North Atlantic. *Ocean Dynamics*, 57:223–235, 2007. doi:10.1007/s1036-007-0104-7.
- 5 Domingues, C. M., Church, J. A., Whie, N. J., Gleckler, P. J., Wijffels, S. E., Barker, P. M., and Dunn, J. R. Improved estimates of upper ocean warming and multidecadal sea level rise. *Nature*, 453:1090–1094, 2008.
- Eden, C. and Willebrand, J. Mechanism of Interannual to Decadal Variability of the North Atlantic Circulation. *Journal of Climate*, 14:2266–2280, 2001.
- 10 Emery, W. J. and Thomson, R. E. *Data Analysis in Physical Oceanography*. Elsevier, 2 edition, 2004.
- Goni, G., Roemmich, D., Molinari, R., Meyers, G., Sun, C., Boyer, T., Baringer, M., , Gouretski, V., DiNezio, P., Reseghetti, F., Vissa, G., Swart, S., Keeley, R., Garzoli, S., Maes, C., and Reverdin, G. The Ship of Opportunity Program. In
15 *Proceedings of OceanObs09:Sustained Ocean Observations and Information for Society (Vol.2)*. ESA Publication WPP-306, 2010.
- Gouretski, V., Kennedy, J., Boyer, T., and Köhl, A. Consistent near-surface ocean warming since 1900 in two largely independent observing networks. *Geophysical Research Letter*, 39(L19606):1–8, 2012.
- 20 Gouretski, V. and Koltermann, K. P. How much is the ocean really warming? *Geophysical Research Letter*, 34(L01610), 2007.
- Gouretski, V. and Reseghetti, F. On depth and temperature biases in bathythermograph data: Development of a new correction scheme based on analysis of a global ocean database. *Deep Sea Research I*, 57:812–833, 2010.

Häkkinen, S. and Rhines, P. B. Shifting surface currents in the northern North Atlantic Ocean. *Journal of Geophysical Research*, 114:1–12, 2009. doi: 10.1029/2008JC004883.

Hanawa, K., Rual, P., Bailey, R., Sy, A., and Szabados, M. A new depth-time
5 equation for Sippican of TSK T-7, T-6 and T-4 expendable bathythermographs.
Deep Sea Research I, 42:1423–1451, 1995.

Ishii, M. and Kimoto, M. Reevaluation of historical Ocean Heat Content Variations with Time-Varying XBT and MBT Depth Bias Corrections. *Journal of Oceanography*, 65:287–299, 2009.

10 Köller, M., Käse, R. H., and Herrmann, P. Interannual to multidecadal variability and predictability of North Atlantic circulation in a coupled earth system model with parametrized hydraulics. *Tellus*, 62A:569–578, 2010. doi:10.1111/j.1600-0870.210.00450.x.

Levitus, S., Antonov, J., and Boyer, T. Warming of the World Ocean, 1955–2003.
15 *Geophysical Research Letters*, 32(L02604):1–4, 2005.

Levitus, S., Antonov, J. I., Boyer, T. P., Baranova, O. K., Garcia, H. E., Locarnini,
R. A., Mishonov, A. V., Reagan, J. R., Seidov, D., Yarosh, E. S., and Zweng, M.
World ocean heat content and thermosteric sea level change (0–2000m), 1955–2010.
Geophysical Research Letters, 39(L10603):1–5, 2012. doi:10.1029/2012GL051106.

20 Lozier, M. S., Leadbetter, S., Williams, R. G., Roussenov, V., Reed, M. S. C., and Moore, N. J. The Spatial Pattern and Mechanisms of Heat-Content Change in the North Atlantic. *Science*, 319:800–803, 2008.

Lyman, J. M. Estimating Global Energy Flow from the Global Upper Ocean.
Surveys in Geophysics, 33:387–393, 2012.

- Lyman, J. M., Willis, J. K., and Johnson, G. C. Recent cooling in the upper ocean. *Geophysical Research Letters*, 33(L18604):1–5, 2006.
- Molinari, R. L. Information from low-density expendable bathythermograph transects: North Atlantic mean temperature structure and quasi-decadal variability. *Progress in Oceanography*, 88:131–149, 2011.
- Olbers, D., Willebrand, J., and Eden, C. *Ocean Dynamics*. Springer Verlag, 1 edition, 2012.
- Palmer, M. D. and Co-Authors. Future Observations for Monitoring Global Ocean Heat Content. In *Proceedings of OceanObs09:Sustained Ocean Observations and Information for Society (Vol.2)*. ESA Publication WPP-306, 2010.
- Palmer, M. D. and Haines, K. Estimating Oceanic Heat Content Change Using Isotherms. *Journal of Climate*, 22:4953–4969, 2009.
- Palmer, M. D., Haines, K., Tett, S. F. B., and Ansell, T. J. Isolating the signal of ocean global warming. *Geophysical Research Letters*, 34(L23610):1–6, 2007.
- Pierce, D. W., Barnett, T. P., and Gleckler, P. J. Ocean Circulations, Heat Budgets, and Future Commitment to Climate Change. *Annual Review of Environment and Resources*, 36:27–43, 2011.
- Robson, J., Sutton, R., Lohman, K., Smith, D., and Palmer, M. Causes of the Rapid warming of the North Atlantic Ocean in the Mid-1990s. *Journal of Climate*, 25, 2012.
- Scott, J. *Expendable Sensors*, volume 2, pages 345–351. Elsevier, Inc., 2 edition, 2009.
- Talley, L. D., Pickard, G. L., Emery, W. J., and Swift, J. H. *Descriptive Physical Oceanography: An Introduction*. Elsevier, Inc, 6 edition, 2011.

- Troupin, C., Barth, A., Sirjacobs, D., Ouberdoos, M., Brankart, J.-M., Brasseur, P., Rixen, M., Alvera-Azcárate, A., Belounis, M., Capet, A., Lenartz, F., Toussaint, M.-E., and Beckers, J.-M. Generation of analysis and consistent error fields using the DataInterpolating Variational Analysis (Diva). *Ocean Modelling*, 52-53:90–101, 2012. doi:10.1016/j.ocemod.2012.05.002.
- Troupin, C., Machn, F., Ouberdoos, M., Sirjacbs, D., Barth, A., and Beckers, J. High-resolution climatology of the northeast atlantic using Data Interpolating Variational Analysis (DIVA). *Journal of Geophysical Research*, 115:1–20, 2010. doi:doi:10.1029/2009JC005512.
- ¹⁰ Vallis, G. K. *Climate and the Oceans*. Princeton University Press, 1 edition, 2012.
- Visbeck, M., Chassignet, E. P., Curry, R. G., Delworth, T. L., Dickson, R. R., and Krahmann, G. The Ocean’s Response to North Atlantic Oscillation Variability. In J. Hurrell, Y. Kushnir, G. Ottersen, and M. Visbeck, editors, *The North Atlantic Oscillation: Climatic Significance and Environmental Impact*, pages 113–145. American Geophysical Union, 2003. doi:10.1029/134GM06.
- Wijffels, S. E., Willis, J., Domingues, C. M., Barker, P., White, N. J., Gronell, A., Ridgway, K., and Church, J. A. Changing Expendable Bathymeterograph fall rates and their impact on estimates of thermosteric sea level rise. *Journal of Climate*, 21:5657–5672, 2008.
- ²⁰ Willis, J. K., Lyman, J. M., Johnson, G. C., and Gilson, J. Correction to "Recent cooling of the upper ocean". *Geophysical Research Letters*, 34(L16601):1, 2007.
- Willis, J. K., Lyman, J. M., Johnson, G. C., and Gilson, J. In Situ Data Biases and Recent Ocean Heat Content Variability. *Journal of Atmospheric and Oceanic Technology*, 26:846–852, 2008.

Zhai, X. and Sheldon, L. On the North Atlantic Heat Content Change between 1955-70 and 1980-95. *Journal of climate*, 25:3619–3628, 2012.

Danksagung